frontiers | Frontiers in Chemical Biology

TYPE Original Research
PUBLISHED 12 August 2025
DOI 10.3389/fchbi.2025.1639096

OPEN ACCESS

EDITED BY
Debbie C. Crans,
Colorado State University, United States

REVIEWED BY
Tiziano Marzo,
University of Pisa, Italy
Aviva Levina,
The University of Sydney, Australia

*CORRESPONDENCE
Christina N. Banti,
cbanti@uoi.gr
Sotiris K. Hadjikakou,
shadjika@uoi.gr

RECEIVED 01 June 2025
ACCEPTED 15 July 2025
PUBLISHED 12 August 2025

CITATION
Banti CN, Lezos F, Hatzidimitriou A and Hadjikakou SK (2025) Carboxymethyl cellulose hydrogel doped with zinc-aspirinate as a multifunctional material: photoprotection, epithelial regeneration, and biocompatibility. *Front. Chem. Biol.* 4:1639096. doi: 10.3389/fchbi.2025.1639096

Carboxymethyl cellulose hydrogel doped with zinc-aspirinate as a multifunctional material: photoprotection, epithelial regeneration, and biocompatibility

Christina N. Banti[1]*, Fotakis Lezos[1], Antonios Hatzidimitriou[2] and Sotiris K. Hadjikakou[1]*

[1]Biological Inorganic Chemistry Laboratory, Department of Chemistry, University of Ioannina, Ioannina, Greece, [2]Laboratory of Inorganic Chemistry, Department of Chemistry, Aristotle University of Thessaloniki, Thessaloniki, Greece

The synthesis of a new Carboxymethyl Cellulose Hydrogel (CMC) doped with Zinc-Aspirinate (**ZnAsp** = $[Zn(Asp)_2(H_2O)_2]$) of formula **CMC@ZnAsp** is reported. The hydrogel **CMC@ZnAsp** and its ingredient **ZnAsp** were characterized by melting point (m.p.) and X-Ray Fluorescence (XRF), Attenuated Total Reflection Fourier-Transform Infrared (ATR-FTIR) and Nuclear Magnetic Resonance (^{1}H-NMR) spectroscopies. The photo-reactivity of **CMC@ZnAsp** and its constituent **ZnAsp** under UVB radiation (λ_{max} = 280 nm) was monitoring using ^{1}H-NMR spectroscopy. The *in vitro* cytotoxicity of both **CMC@ZnAsp** and **ZnAsp** was assessed against immortalized human keratinocyte (HaCaT) cells. Their potential role in promoting wound healing—specifically, the growth and migration of new epithelial cells to restore the integrity of the skin—was investigated using a scratch assay on HaCaT cells. Furthermore, the *in vitro* anti-inflammatory activity of **CMC@ZnAsp** and **ZnAsp** was also examined. Their *in vivo* toxicity was evaluated by *Artemia salina* assay.

KEYWORDS

biological inorganic chemistry, zinc, hydrogel, epithelial regeneration, toxicity

Introduction

Epidermis serves as a protective barrier against solar UV radiation (de Szalay and Wertz, 2023). However, prolonged exposure to UV radiation can impair this barrier function in human skin (Biniek et al., 2012). Consequently, sun protection is widely employed to safeguard the skin, as it helps prevent sunburns, skin cancer, photoaging, and the various inflammatory effects caused by solar radiation (Agostino et al., 2020). This is why photoprotective topical products, contain effective sun-blocking agents and often include combinations of active ingredients to enhance protection (Kaur and Saraf, 2023). The chemical properties of photoprotective materials include non-irritating, chemically inert, photostable, and possessing antioxidant activity (Kockler et al., 2012). Inorganic

oxides such as ZnO or TiO_2 and systemic protectants have been explored as potential photoprotective (Smijs and Pavel, 2011). Classical sunscreens rely primarily on light-scattering and semiconductor properties, particularly of ZnO and TiO_2 nanoparticles (Smijs and Pavel, 2011). However, ZnO, on the other hand, has been specifically approved by the US FDA as a Category I protectant and is considered safe, with anti-irritant, astringent, and skin-healing properties although possess no light-scattering and semiconductor properties (Gadgil et al., 2023). Therefore, an alternative multifunctional approach to photoprotection—combining photostability, anti-inflammatory activity, and the promotion of epithelial regeneration, rather than relying solely on UV absorption or scattering—may represent a promising strategy worthy of further investigation (Palem et al., 2024). Moreover, one of the key challenges in photoprotective materials development is ensuring human safety by preventing penetration through the skin barrier (Aguilera et al., 2023). To achieve this, hydrogels can be developed to enhance stability, reduce skin permeability, and ensure a uniform distribution of UV filters across the skin barrier (Aguilera et al., 2023; Lu et al., 2024). Hydrogels are three-dimensional network structures, characterized by high water content, strong skin adhesion, antioxidant properties, and a cooling effect. The incorporation of polysaccharide-based components, such as cellulose nanocrystals, enables the formation of hydrogels that prevent penetration across the skin barrier (Aguilera et al., 2023).

As part of our ongoing efforts to develop new therapeutic formulations (Sainis et al., 2016; Banti et al., 2017; Banti et al., 2021; Karetsi et al., 2019; Stathopoulou et al., 2018) with minimal photoreactivity, and strong antioxidant properties, we report here the synthesis and characterization of the hydrogel of formula **CMC@ZnAsp**, (CMC = carboxymethyl cellulose) which contains the known zinc(II) complex [Zn $(asp)_2(H_2O)_2$] (**ZnAsp**). The photoreactivity of **CMC@ZnAsp** and its constituent **ZnAsp** under UVB radiation (λ_{max} = 280 nm) was evaluated by irradiating the samples for 6 h and monitoring them using ^{1}H-NMR spectroscopy. The *in vitro* cytotoxicity of both **CMC@ZnAsp** and **ZnAsp** was assessed against immortalized human keratinocyte (HaCaT) cells. Their potential role in promoting wound healing—specifically, the growth and migration of new epithelial cells to restore the integrity of the skin or mucosal surfaces—was investigated using a scratch assay on HaCaT cells. Furthermore, their *in vitro* anti-inflammatory activity was also examined. The *in vivo* toxicity was evaluated by *Artemia salina* assay.

Results and discussion

General aspects: The hydrogel **CMC@ZnAsp** was prepared by incorporating **ZnAsp** (13.3% w/w) into a CMC (86.7% w/w) matrix. Its characterization was carried out using XRF, ATR-FTIR, UV-Vis, and ^{1}H NMR spectroscopies. **ZnAsp** was synthesized by reacting $Zn(NO_3)_2{\cdot}6H_2O$, KOH, and aspirin in a 1:1:1 M ratio in 5 mL of double deionized water (ddH_2O). The resulting suspension was centrifuged, and crystals were obtained from the supernatant. **ZnAsp** was characterized by X-ray diffraction analysis. Its unit cell parameters are: space group: C2/c; a = 25.353 (3), b = 7.1820 (8), c = 11.1231 (13) Å, β = 108.078 (3)°, R = 0.0266. These parameters are identical with those reported earlier (space group: Cc; a = 25.345 (4), b = 7.201 (2), c = 11.137 (5) Å, β = 108.02 (3)°, R = 0.043 (Hartmann and Vahrenkamp, 1994), space group: C2/c; a = 25.345, b = 7.201, c = 11.137 Å, β = 108.02° (Marsh, 2004), and space group: C2/c; a = 25.385 (2), b = 7.192 (4), c = 11.137 (5) Å, β = 108.07 (4)°, R = 0.0315 (Lemoine et al., 2004). Since the quality of the **ZnAsp** crystals obtained in this study was suitable for X-ray crystallographic analysis and given that the previously reported structures exhibited high R values, we proceeded with the full solution and refinement of the diffraction data for **ZnAsp**. The composition of the bulk of the sample was identified to correspond to the crystal structure using melting point and XRF, ATR-FTIR, UV-Vis, and ^{1}H NMR spectroscopies.

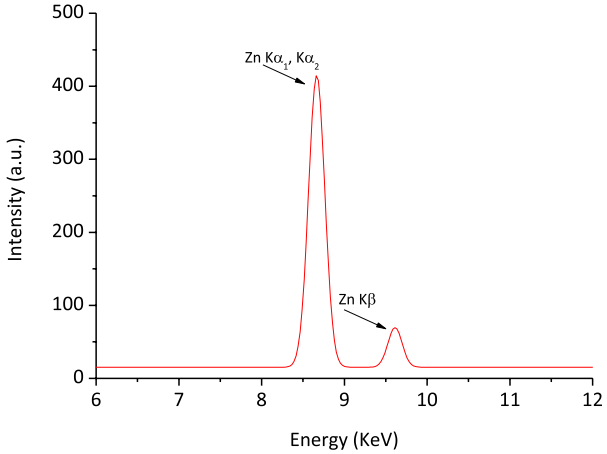

FIGURE 1
XRF spectrum of **CMC@ZnAsp**.

Solid state studies

X-ray fluorescence spectroscopy: The XRF spectrum confirms the presence of Zn in the **CMC@ZnAsp** hydrogel (Figure 1). The zinc content was determined to be 3.3%. By assuming that the dry hydrogel contains only the added components without any residual water, the incorporation of 0.00732 g of **ZnAsp** (containing 14.2% Zn) to 0.02 g of CMC yields a theoretical zinc content of 3.8% in **CMC@ZnAsp**.

Crystal and molecular structure of ZnAsp: The crystal and molecular structure of **ZnAsp** is shown in Figure 2. While the structure of **ZnAsp** has been previously reported, in this work we provide a more precise refinement and verify its chemical formulation (Hartmann and Vahrenkamp, 1994; Lemoine et al., 2004; Marsh, 2004).

Solution state studies

^{1}H-NMR spectroscopy: The ^{1}H-NMR spectrum of **CMC@ZnAsp** was recorded in D_2O and compared with that of **ZnAsp** (Figure 3). The singlet signal at 1.905 ppm of **CMC@ZnAsp** is

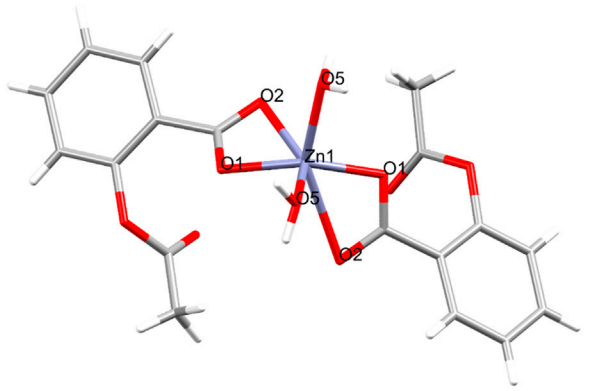

FIGURE 2
Molecular structure of **ZnAsp**. Selected bond lengths [Å] and angles [°]: Zn1-O1 = 1.9838 (16), Zn1-O2 = 2.5280 (18), Zn1-O5 = 2.0128 (15), Zn1-O1_a = 1.9838 (16), Zn1-O2_a = 2.5280 (18), Zn1-O5_a = 2.0128 (15), O1-Zn1-O2 = 56.29 (6), O1-Zn1-O5 = 112.95 (6), O1-Zn1-O1_a = 135.21 (6), O1-Zn1-O2_a = 96.28 (6), O1-Zn1-O5_a = 98.20 (6), O2-Zn1-O5 = 86.89 (6).

assigned to the methyl protons of aspirin which is in accordance with the corresponding -CH_3 group of **ZnAsp** which also appeared at 1.951 ppm. The resonance signals of **CMC@ZnAsp** at 6.936–6.868 (t, H^b aromatic), 7.413–7.361 (t, $H^{d,e}$ aromatic) and 7.771–7.739 (d, H^f aromatic) are in agreement with those dominated in initial compound **ZnAsp** (6.913–6.844 (t, aromatic H^b), 7.406–7.344 (t, aromatic $H^{d,e}$) and 7.754–7.723 (d, aromatic H^f)) (Figure 3). Moreover, the resonance signals of CMC are observed at 4.246–3.161 ppm (Kono et al., 2016; Stathopoulou et al., 2018) (Figure 3).

Stability of ***ZnAsp*** *or* ***CMC@ZnAsp*** in double distilled water (ddw) solutions: Stability of **ZnAsp** or **CMC@ZnAsp** in ddw solutions was assessed using UV-Vis spectroscopy. Figure 4 presents the absorption spectra of **ZnAsp**, **CMC@ZnAsp**, **Aspirin** and **Salicylic acid**. These data indicate that the solid-state structure of **ZnAsp** is preserved in solution, whether as the free complex or when dispersed within CMC (**CMC@ZnAsp**). A similar conclusion was drawn when the corresponding spectra were recorded in phosphate-buffered saline (PBS, pH 7), representative of cell culture conditions. Stability was also evaluated under mildly acidic conditions, mimicking healthy skin (pH 4.5–5.5), using a sodium acetate buffer at pH 5.5 (Figure 4). The results confirmed that the structural integrity of the complex was retained in all tested media—double-distilled water (ddw), PBS, and sodium acetate buffer solution (SABS). Chiaverini et al. (2024) showed that the $Mo_2(Asp)_4$ complex maintains its structural stability longer than other $Mo_2(NSAID)_4$ analogues, while still undergoing controlled disassembly in biological environments to release active components. This dual behavior supports its potential as a therapeutic candidate, especially in applications requiring targeted and sustained release of NSAIDs. Moreover, the synthesis of the **CMC@ZnAsp** hydrogel involves dissolving **ZnAsp** in water with the simultaneous addition of the appropriate amount of CMC. The process lasts approximately 3 h. The UV-Vis spectrum of the hydrogel containing **CMC@ZnAsp**, recorded after this period, is identical to that of the free **ZnAsp** complex recorded immediately after its preparation (Figure 4).

Ultraviolet Protection Factor (UPF) of ***ZnAsp*** *and* ***CMC@ZnAsp***: The UV-protective properties of **ZnAsp** and **CMC@ZnAsp** were evaluated according to standard techniques aligned with ISO 23675 principles. A solution of **ZnAsp** (5×10^{-4} M) or **CMC@ZnAsp** (5×10^{-4} M in respect of **ZnAsp**) was prepared, and its absorbance was measured across the UV range of 290–400 nm (UVA and UVB radiation) using a UV-Vis spectrophotometer. The absorbance values were converted to % transmittance (T%), and a transmittance spectrum (T% vs. wavelength) was generated (Figure 5).

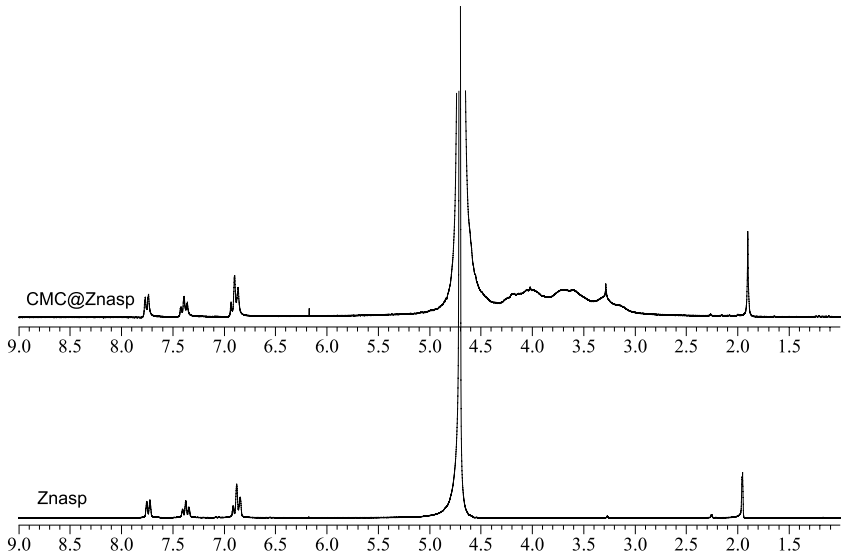

FIGURE 3
^{1}H-NMR spectra of **CMC@ZnAsp** and **ZnAsp** in D_2O.

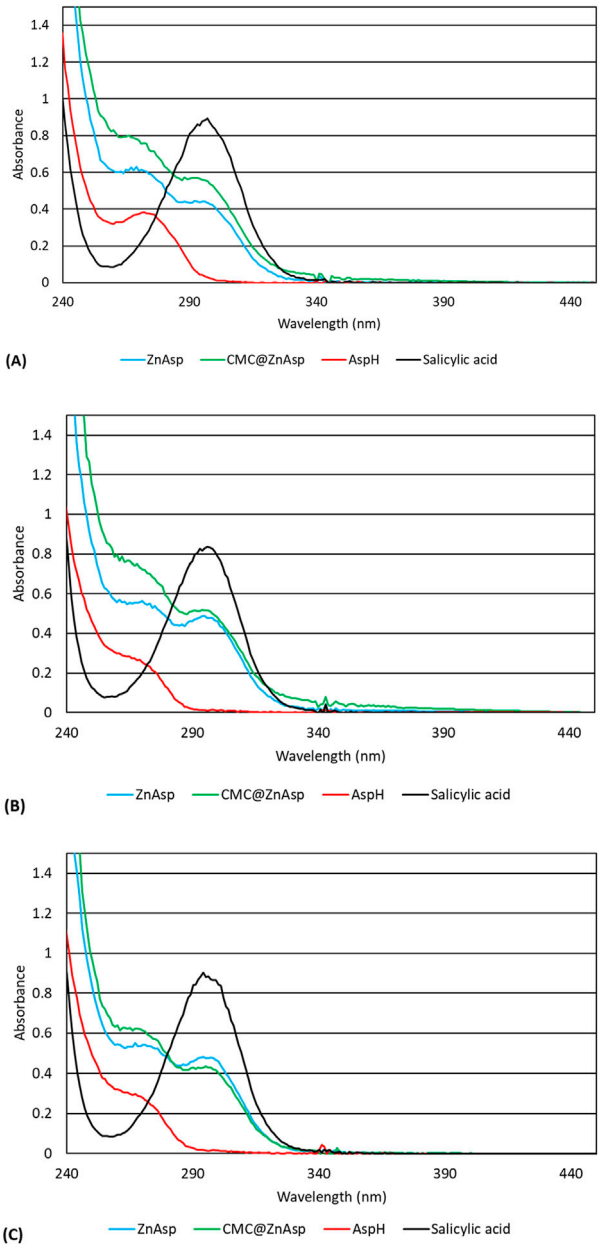

FIGURE 4
UV spectra of **ZnAsp** (5×10^{-4} M), **CMC@ZnAsp** (5×10^{-4} M), Asp (5×10^{-4} M), $SalH_2$ (2.5×10^{-4} M) in ddH_2O **(A)**, PBS **(B)** and 0.05M sodium acetate pH 5.5 **(C)**.

To quantify the protective effect, the surface area under the T% vs. wavelength curve was calculated. Ultraviolet Protection Factor (UPF) determination was performed by calculating the quotient of the surface integrals of transmittance multiplied by wavelength, over the 290–400 nm range, without and with the Zn-aspirinate solution:

$$\mathrm{UPF} = \frac{\int_{290}^{400} T_{\mathrm{ref}}(\%) \cdot d\lambda}{\int_{290}^{400} T_{\mathrm{ZnAsp}}(\%) \cdot d\lambda}$$

where T_{ref} is the transmittance without **ZnAsp** or **CMC@ZnAsp** and T_{ZnAsp} or $T_{CMC@ZnAsp}$ is the transmittance of the **ZnAsp** or **CMC@ZnAsp** solution.

This value was subsequently normalized to a standard application density of 2 mg/cm^2, as required for consistent comparison with standard protective formulations.

The resulting UPF values of the ZnAsp and CMC@ZnAsp solutions were **9.85** and **11.05**, respectively, indicating **moderate UV protection** in both cases. These results demonstrate that the **CMC@ZnAsp hydrogel exhibits a higher UPF** compared to its **ZnAsp** component alone. Furthermore, the hydrogel's enhanced ability to absorb and attenuate UV radiation across both the UVA and UVB radiations highlights its potential for use in formulations designed for effective UV shielding.

Continuous photolysis: Photostability under sun exposure or ultraviolet (UVB) radiation is essential to ensure the effectiveness and safety of commercial sunscreens (Gonzalez et al., 2007). While the average daily outdoor exposure is typically 1–2 h, this can increase substantially to 5–6 h during holidays (Diffey, 2011). In light of this, we evaluated the photostability of both **CMC@ZnAsp and ZnAsp** under UVB radiation (λ_{max} = 280 nm) in D_2O solution for a continuous 6-h period. The reaction was monitored using ^{1}H-NMR spectroscopy (Supplementary Figure S1). No changes were detected between the initial spectra of **CMC@ZnAsp** or **ZnAsp** and those recorded after UVB exposure, indicating that both the hydrogel **CMC@ZnAsp** and its **ZnAsp** component remain stable without undergoing decomposition. This photostability supports their potential use in photoprotective hydrogel formulations.

In Vitro Toxicity against Immortalized Human Keratinocytes (HaCaT) Cells: To assess the toxicity of **CMC@ZnAsp** and **ZnAsp**, HaCaT cells were chosen as a representative model for studying the cellular pharmacokinetics of compounds in keratinocytes (Pessina, et al., 2001). HaCaT cells are useful for testing preventive and therapeutic strategies for skin-related conditions (Tyagi et al., 2015). The cells screening performed using the sulforhodamine B (SRB) assay. HaCaT cells were incubated with **CMC@ZnAsp**, and **ZnAsp** for 48 h. The IC_{50} value for **CMC@ZnAsp** is 80.0 ± 2.4 μM, while the corresponding value for **ZnAsp** is 83.3 ± 2.4 μM. Moreover, **CMC@Znasp** and **ZnAsp** were irradiated with UVB light for a period of 6 h and the HaCaT cells were incubated with the radiated, **CMC@Znasp** and **ZnAsp**. The IC_{50} values of the radiated **CMC@Znasp** and **ZnAsp** are 72.6 ± 0.8 and 84.4 ± 2.1 μM, respectively. Thus, both **CMC@ZnAsp** and **ZnAsp**, along with their UV-irradiated counterparts, exhibited similar levels of toxicity towards HaCaT cells, indicating good photostability and low cytotoxicity for the hydrogel **CMC@ZnAsp** and its active component **ZnAsp**.

In vivo toxicity evaluation by brine shrimp A. salina: The zooplanktonic crustacean *A. salina* is used as a model organism for *in vivo* toxicological testing by the U.S. Environmental Protection Agency (EPA) (Banti and Hadjikakou, 2021). The *A. salina* assay is closely correlated with toxicity data from rodent and human studies and is commonly used to assess the *in vivo* toxicity of the hydrogel, its active ingredient, and its photoproducts (Banti and Hadjikakou, 2021).

The survival rates (%) of *A. salina* larvae were assessed at a concentration of 50 μM, which corresponds to the concentration used for evaluating keratinocyte cell migration in the *in vitro* scratch wound assay (see below). Additionally, higher concentrations of 90, 180, and 360 μM were tested after a 24-h incubation period. No toxic effects on the survival of *A. salina* were observed for the **CMC@ZnAsp** hydrogel and **ZnAsp**, or their corresponding irradiated **CMC@ZnAsp** and **ZnAsp**, indicating that both the **CMC@ZnAsp** and **ZnAsp** and their irradiated counterparts are non-toxic.

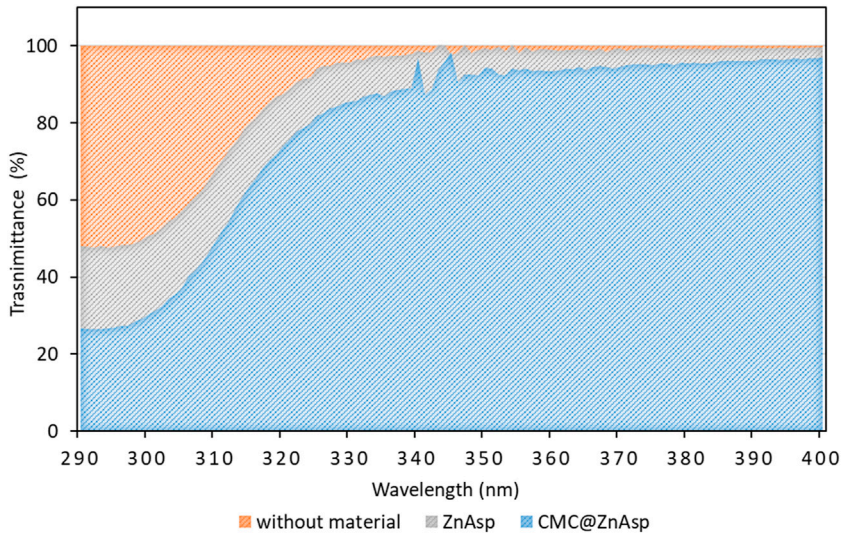

FIGURE 5
Ultraviolet Protection Factor (UPF) determination as the quotient of the surface areas ($\int_{290}^{400} T(\%)*\lambda\ (nm)\, d\lambda$) without and with **the CMC@ZnAsp** and **ZnAsp**.

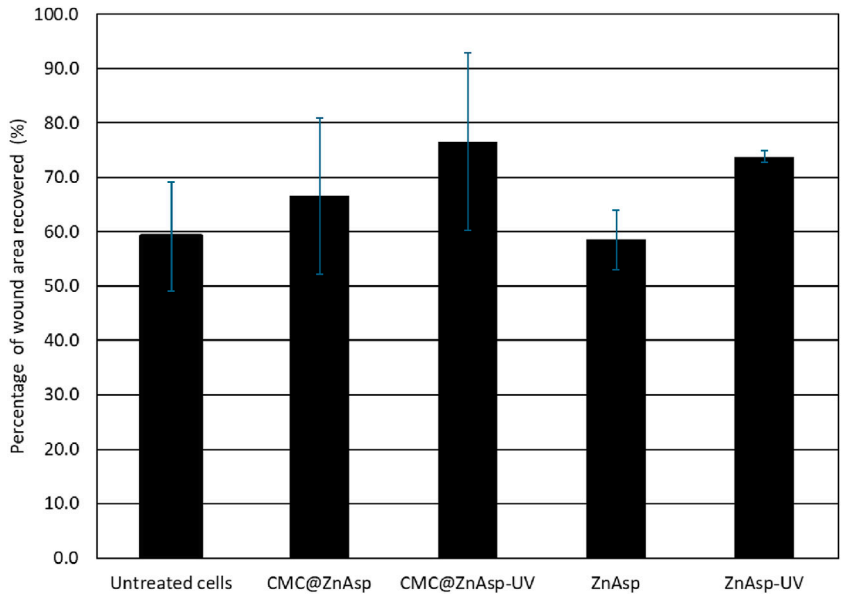

FIGURE 6
Histogram showing the RWA % of untreated or treated cells with **CMC@ZnAsp** or **ZnAsp** and their irradiated counterparts at 50 μM after 48 h incubation (mean values are: untreated: 59.1%, **CMC@ZnAsp**: 66.6%, **CMC@ZnAsp**-UV: 76.5%, **ZnAsp**: 58.6% and **ZnAsp**-UV: 73.8% respectively). Error bars indicate confidence limits with alpha value = 0.05 (untreated: ±10%, **CMC@ZnAsp**: ±14.3%, **CMC@ZnAsp**-UV: ±16.3%, **ZnAsp**: ±5.5% and **ZnAsp**-UV: ±1.1% respectively). Mean Values and confidence limits were determined from 4 independent experiments.

Anti-inflammation activity by albumin denaturation assay: The anti-inflammatory activity of **CMC@ZnAsp** and **ZnAsp** was initially assessed *in vitro* using the albumin denaturation assay. This assay measures the inhibition of protein denaturation, specifically the disruption of its secondary and tertiary structures (Chick, et al., 2025). Generally, protein denaturation is a critical pathological process associated with inflammation and conditions such as rheumatoid arthritis (Rajamohan et al., 2025). The non steroidal anti-inflammatory drug, diclofenac was used for a standard positive control (Chick, et al., 2025). The IC_{50} value of diclofenac is 2.45 ± 0.50 mM. **ZnAsp** demonstrated a stronger effect, with a calculated IC_{50} value of 1.96 ± 0.26 mM, indicating significant anti-inflammatory activity by effectively inhibiting protein denaturation—surpassing the activity of diclofenac sodium.

Migration of keratinocytes in wound margin by in vitro scratch wound assay: Self-healing properties are essential to the effectiveness of the formulated hydrogel sunscreens (Heydari et al., 2025). The re-

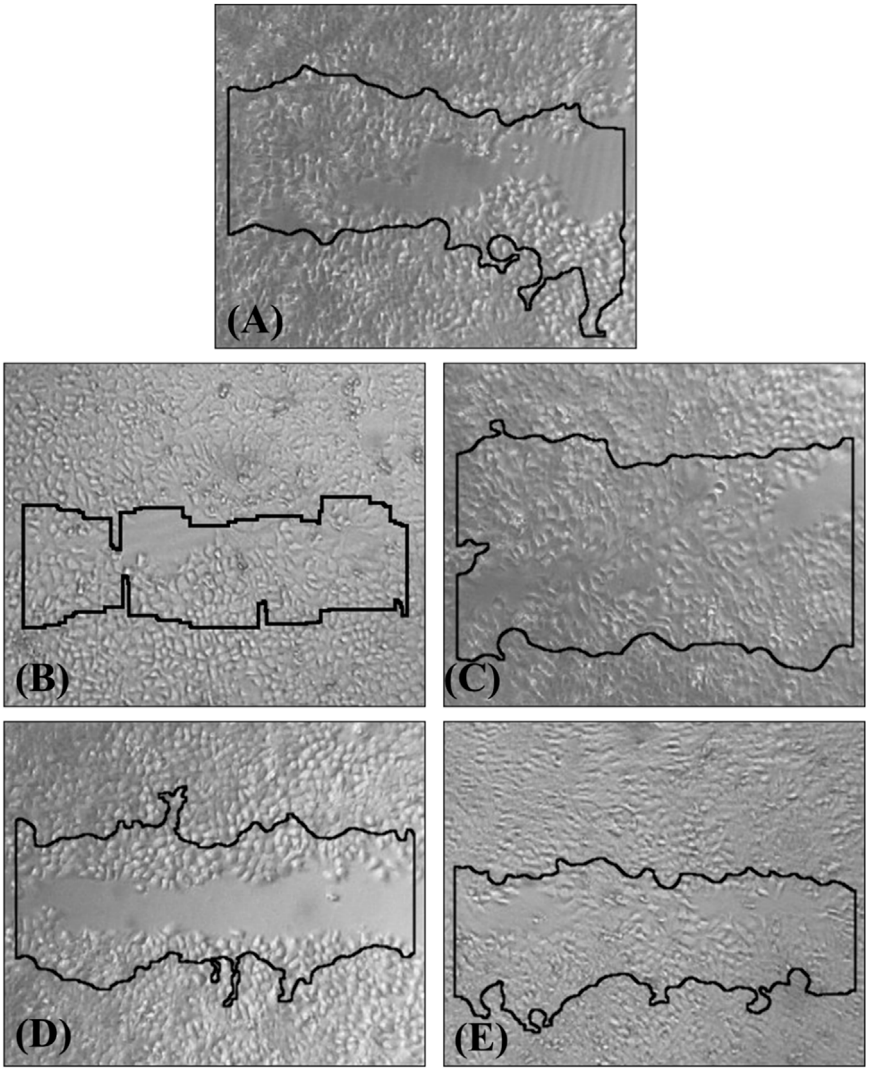

FIGURE 7
HaCaT cell wound healing at 48 h, relative to the initial wound (0 h, solid line): **(A)** in untreated cells, **(B) CMC@ZnAsp**, **(C)** irradiated **CMC@ZnAsp**, **(D) ZnAsp** and **(E)** irradiated of **ZnAsp** at 50 μM.

epithelialization process is a critical phase of wound healing, during which cells migrate from the wound margins toward the center to facilitate ulcer closure (Stathopoulou et al., 2018).

The *in vitro* scratch wound assay is based on creating an artificial gap, or "scratch," on a confluent cell monolayer. The cells migrate toward the gap, healing the wound by combining migration and proliferation (Stathopoulou et al., 2018).

The effects of the hydrogel, its ingredients, and their photoproducts on cell migration were evaluated after 48 h of incubation with HaCaT cells (Figures 6, 7). The tested concentration of 50 μM can be considered non-cytotoxic, as the cells' viability at this level exceeds 70%. According to FDA ISO 10993-5 that regulates the "Biological evaluation of medical devices - Part 5: Tests for *in vitro* cytotoxicity," if the percent of viability is higher than 70% upon treatment with an agent, this agent is considered as noncytotoxic. in accordance with ISO 10993-5, which regulates the Biological evaluation of medical devices–Part 5: Tests for *in vitro* cytotoxicity (Banti et al., 2023).

The recovered wound area (RWA %) is defined as:

$$\mathrm{RWA}\,(\%) = 100^{*}\frac{\text{initial wound area} - \text{final wound area}}{\text{initial wound area}}$$

Upon 48 h incubation, the RWA % was 59.1% in the untreated keratinocytes, on the contrary of 66.7% of **CMC@ZnAsp**, and 76.5% of the irradiated **CMC@ZnAsp**, 58.6% of the **ZnAsp**, and 73.8% of the irradiated of **ZnAsp**, suggesting that **CMC@ZnAsp** and **ZnAsp** as well as their counterparts show wound healing properties towards HaCaT cells after 48 h incubation at the concentration of 50 μM.

Conclusion

In this study, we successfully synthesized and characterized a novel biocompatible hydrogel, **CMC@ZnAsp**, incorporating the zinc(II)-aspirinate complex [Zn $(asp)_2(H_2O)_2$] (**ZnAsp**). The hydrogel and **ZnAsp** were fully characterized using spectroscopic and

crystallographic techniques. Notably, both **CMC@ZnAsp** and **ZnAsp** exhibited excellent photostability under UVB radiation, as evidenced by unchanged ^{1}H-NMR spectra following prolonged irradiation.

Biological assessments confirmed the low cytotoxicity of both formulations against human keratinocytes (HaCaT cells), with IC_{50} values above 70 μM, even after UV exposure. Furthermore, *in vivo* toxicity testing using *A. salina* demonstrated the non-toxic nature of the hydrogel and its constituents, even at elevated concentrations. Importantly, both **CMC@ZnAsp** and **ZnAsp** significantly promoted keratinocyte migration in an *in vitro* scratch wound assay, highlighting their potential in epithelial regeneration. Their anti-inflammatory activity, demonstrated via the BSA denaturation assay, further supports their therapeutic relevance.

Collectively, our results demonstrate that **CMC@ZnAsp** is a safe, photostable, and multifunctional hydrogel with promising applications in photoprotection, wound healing, and anti-inflammatory therapies.

Experimental

Materials and instruments: All solvents used were of reagent grade. Dulbecco's modified Eagle's medium, (DMEM), fetal bovine serum and penicillin–streptomycin were purchased from Gibco, Glasgow, United Kingdom. Phosphate buffer saline (PBS) was purchased from Sigma-Aldrich. Trypsin–EDTA and L-glutamine were purchased from Biowest. Sulforhodamine B was purchased from Alfa Aesar. Melting points were measured in open tubes with a Stuart Scientific apparatus and are uncorrected. Mid-infrared spectra (4000–400 cm^{-1}) were obtained on a Cary 670 FTIR spectrometer (Agilent Technologies). The ^{1}H-NMR spectra were recorded on a Bruker AC 400 MHz FT-NMR instrument in D_2O solution. XRF measurement was also carried out with a Rigaku NEX QC EDXRF analyser (Austin, TX, United States). For the toxicity experiments, brine shrimp eggs (*A. salina*) were purchased from Ocean Nutrition. Sea salt was purchased from Tropic Marin. HaCaT cells were obtained from the American Type Culture Collection (ATCC, Rockville, MD, United States).

Synthesis and crystallization of **ZnAsp**: Solution of 0.5 mmol of aspirin (0.090 g) were stirred in ddw (5 mL) for 30 min and it was treated with 0.5 mL of KOH 1N, stirred for 30 min and then a clear solution of 1 mmol $Zn(NO_3)_2{\cdot}6H_2O$ (0.300 g) was added. The solution was mixed for 40 min and it was centrifuged for 20 min at 5000 rpm. Afterwards, from the supernatant of the above solution, white-grey crystals suitable for X-ray analysis were grown from slow evaporation of the solution.

ZnAsp: $C_{18}H_{18}O_{10}Zn$, White-grey crystal, melting point: 87–89 °C; elemental analysis found: C: 47.52; H: 3.90, Zn = 14.59%. calculated for $C_{18}H_{18}O_{10}Zn$: C: 47.04; H: 3.94, Zn: 14.22%. IR (cm^{-1}): 3333 (br), 3052 (br), 1733 (s), 1591 (s), 1557 (s), 1484 (m), 1450 (m), 1402 (vs.), 1224 (vs.), 1196 (vs.), 1097 (s), 1037 (m), 1011 (m), 926 (m), 871 (m), 824 (m), 756 (m), 714 (m), 684 (w), 654 (w), 543 (w), 509 (w), 480 (m); ^{1}H-NMR (ppm) in D_2O: 6.913–6.844 (t, aromatic H^b), 7.406–7.344 (t, aromatic $H^{d,e}$), 7.754–7.723 (d, aromatic H^f), 1.951 (s, CH_3 group).

Synthesis of the hydrogel with carboxymethyl cellulose (CMC): The hydrogel **CMC@ZnAsp** were synthesized according to following method: 2 mL aqueous solutions of **ZnAsp** 10^{-2} M and 0.04 gr of CMC (2% CMC) were mixed and stirred until complete gelation (Stathopoulou et al., 2018). The resulting composite is clear. The tubes with the hydrogel were stored in darkness sealed at room temperature.

X-ray Structure Determination: Single crystals of **ZnAsp** suitable for crystal structure analysis were obtained by slow evaporation of their mother liquids at room temperature. They were mounted at room temperature on a Bruker Kappa APEX2 diffractometer equipped with a Triumph monochromator using Mo Kα radiation. Unit cell dimensions were determined and refined by using the angular settings of at least 200 high-intensity reflections (>10 σ(I)) in the range $2.9 < 2\theta < 27.2°$. Intensity data were recorded using φ and ω scans. All crystals presented no decay during the data collection. The frames collected for each crystal were integrated with the Bruker SAINT Software package (Apex2Version 2 User Manual, 2006) using a narrow-frame algorithm. Data were corrected for absorption using the numerical method (SADABS) based on crystal dimensions (SADABS: Area–Detector Absorption Correction, 1996). The structures were solved using the SUPERFLIP package (Palatinus and Chapuis (2007) incorporated in Crystals. Data refinement (full-matrix least-squares methods on F^2), and all subsequent calculations were carried out using the Crystals version 14.40b program package All nonhydrogen atoms were refined anisotropically. Hydrogen atoms were located by difference maps at their expected positions and refined using soft constraints. By the end of the refinement, they were positioned geometrically using riding constraints to bonded atoms. Crystallographic data (excluding structure factors) for the structure reported in this paper has been deposited with the Cambridge Crystallographic Data Centre as supplementary publication nos. CCDC 2455619. Copies of the data can be obtained free of charge on application to CCDC, 12 Union Road, Cambridge CB2 1EZ, United Kingdom (fax: (+44) 1223–336-033; e-mail: deposit@ccdc.cam.ac.uk).

ZnAsp: $C_{18}H_{18}O_{10}Zn$, MW = 459.71, monoclinic, space group *C2/c*, a = 25.353 (3), b = 7.1820 (8), c = 11.1231 (13) Å, β = 108.078 (3)°, V = 1925.4 (4) $Å^3$, Z = 4, ρ(calc) = 1.586 g cm^{-3}, μ = 1.330 mm^{-1}, F (000) = 944. 8258 reflections measured, 1796 unique (Rint = 0.035). The final R1 = 0.0266 (for 1598 reflections with I > 2s(I)) and wR (F2) = 0.0586 (all data) S = 1.00.

Photolysis studies: A TUV 15 W G15 T8 low-pressure mercury vapour discharge lamp with a tubular glass envelope UVC lamp, 15 W, manufactured by Phillips was used for the photolysis. The photolysis was performed as follows: Solution of **CMC@ZnAsp** and **ZnAsp** at 10^{-2} M in ddw, was kept in a 1 cm quartz cell under aerobic conditions and the solution was irradiated with ultraviolet light for 6 h. The cell was placed at a distance of 20 cm from the UV source (Banti et al., 2014; Banti et al., 2017).

Biological tests

Solutions of **CMC@ZnAsp** and **ZnAsp** for biological assays were freshly prepared by dissolving the hydrogel material or complex directly in ddw or cell culture medium (DMEM) at the desired low concentrations. Under these dilute conditions, no gelation occurred, and the material behaved as a solution suitable for biological testing. The scratch test and the cell viability assessment by SRB assay were carried out using H_2O/DMEM for **CMC@ZnAsp** and **ZnAsp**.

SRB assay: Solutions of **CMC@ZnAsp** and **ZnAsp** (0.01 M) in ddH_2O were freshly prepared and diluted with the cell culture medium to the desired concentration (5–150 μM). This study was performed as previously reported (Banti et al., 2023).

In vitro scratch wound healing assay: HaCaT cells were grown at a density of 80,000 cells/well for 24 h on a 24-well plate. The next day, shaped wounds were made using a sterile 10 μL pipette tip to scrape across each well, creating a cell free-area. Then, the cells were washed with PBS. The cells were exposed to **CMC@Znasp**, **Znasp** and their irradiated counterparts for 6 hours-at 50 μM in culture medium. Cells for the negative control were also scratched, washed. The scratch closure was monitored for 48 h using phase-contrast microscopy. The scratch area was measured using the ImageJ software (Stathopoulou et al., 2018).

In vivo toxicity evaluation by brine shrimp A. salina: The brine shrimp assay was performed as previously reported (Banti et al., 2023).

Anti-inflammation activity by albumin denaturation assay: The samples were screened for anti-inflammatory properties using the inhibition of albumin denaturation assay, as previously described (Chaiya et al., 2022; Chavan and Hosamani, 2018; Chick et al., 2025). The mixture (2.5 mL) consisted of 0.1 mL of egg albumin (from fresh chicken's egg), 1.4 mL of phosphate buffered saline (PBS, pH 6.4) and 1 mL of varying concentrations of diclofenac sodium or **ZnAsp** (0.4–4.0 mM) in ddH_2O. The double-distilled water served as negative control. Then the mixtures were incubated at 37 °C in an incubator for 15 min and then heated at 70 °C for 5 min. After cooling for 10 min, the absorbance of the samples was measured at 660 nm. The anti-inflammatory activity was estimated as the percentage inhibition or clearance of protein denaturation and calculated according A_{sample} is the absorbance of the test sample (albumin-mixed PBS solution with tested agent) towards $A_{control}$ is the absorbance of the control (albumin-mixed PBS solution without tested compound). The mean values and confidence limits are determined by independent experimental replicates.

Data availability statement

The raw data supporting the conclusions of this article will be made available by the authors, without undue reservation.

Ethics statement

Ethical approval was not required for the studies on human cell in accordance with the local legislation and institutional requirements because only commercially available established cell lines were used.

Author contributions

CB: Investigation, Methodology, Writing – original draft, Writing – review and editing. FL: Investigation, Writing – original draft. AH: Investigation, Methodology, Writing – original draft. SH: Conceptualization, Methodology, Supervision, Validation, Writing – original draft, Writing – review and editing.

Funding

The author(s) declare that no financial support was received for the research and/or publication of this article.

Conflict of interest

The authors declare that the research was conducted in the absence of any commercial or financial relationships that could be construed as a potential conflict of interest.

The author(s) declared that they were an editorial board member of Frontiers, at the time of submission. This had no impact on the peer review process and the final decision.

Generative AI statement

The author(s) declare that no Generative AI was used in the creation of this manuscript.

Publisher's note

Supplementary material

The Supplementary Material for this article can be found online at: https://www.frontiersin.org/articles/10.3389/fchbi.2025.1639096/full#supplementary-material

References

Agostino, S., Azzali, A., Casali, L., Taddei, P., and Grepioni, F. (2020). Environmentally friendly sunscreens: mechanochemical synthesis and characterization of β-CD inclusion complexes of avobenzone and octinoxate with improved photostability. *ACS Sustain. Chem. Eng.* 8, 13215–13225. doi:10.1021/acssuschemeng.0c02735

Aguilera, J., Gracia-Cazaña, T., and Gilaberte, Y. (2023). New developments in sunscreens. *Photochem Photobiol. Sci.* 22, 2473–2482. doi:10.1007/s43630-023-00453-x

Apex2, Version 2 User Manual (2006). *M86–E01078; bruker analytical X-ray systems*. Madison, WI: Inc.

Banti, C. N., Giannoulis, A. D., Kourkoumelis, N., Owczarzak, A., Kubicki, M., and Hadjikakou, S. K. (2014). Novel metallo-therapeutics of the NSAID naproxen. Interaction with intracellular components that leads the cells to apoptosis. *Dalton Trans.* 43, 6848–6863. doi:10.1039/c3dt53175a

Banti, C. N., and Hadjikakou, S. K. (2021). Evaluation of toxicity with brine shrimp assay. *Bio-protocol* 11, e3895. doi:10.21769/bioprotoc.3895

Banti, C. N., Kapetana, M., Papachristodoulou, C., Raptopoulou, C., Psycharis, V., Zoumpoulakis, P., et al. (2021). Hydrogels containing water soluble conjugates of silver(I) ions with amino acids, metabolites or natural products

for non infectious contact lenses. *Dalton Trans.* 50, 13712–13727. doi:10.1039/d1dt02158c

Banti, C. N., Kourkoumelis, N., Tsiafoulis, C. G., Skoulika, S., and Hadjikakou, S. K. (2017). Silver(I) complexes of methyl xanthate against human adenocarcinoma breast cancer cells. *Polyhedron* 121, 115–122. doi:10.1016/j.poly.2016.09.056

Banti, C. N., Papatriantafyllopoulou, C., Papachristodoulou, C., Hatzidimitriou, A. G., and Hadjikakou, S. K. (2023). New apoptosis inducers containing anti-inflammatory drugs and pnictogen derivatives: a new strategy in the development of mitochondrial targeting chemotherapeutics. *J. Med. Chem.* 66, 4131–4149. doi:10.1021/acs.jmedchem.2c02126

Biniek, K., Levi, K., and Dauskardt, R. H. (2012). Solar UV radiation reduces the barrier function of human skin. *Proc. Natl. Acad. Sci. U.S.A.* 109, 17111–17116. doi:10.1073/pnas.1206851109

Chaiya, P., Senarat, S., Phaechamud, T., and Narakornwit, W. (2022). *In vitro* anti-inflammatory activity using thermally inhibiting protein denaturation of egg albumin and antimicrobial activities of some organic solvents. *Mater. Today Proc.* 65, 2290–2295. doi:10.1016/j.matpr.2022.04.916

Chavan, R. R., and Hosamani, K. M. (2018). Microwave-assisted synthesis, computational studies and antibacterial/anti-inflammatory activities of compounds based on coumarin-pyrazole hybrid. *R. Soc. Open Sci.* 5, 172435. doi:10.1098/rsos.172435

Chiaverini, L., Notarstefano, V., Tolbatov, I., Umari, P., Giorgini, E., Ciccone, L., et al. (2024). Dimolybdenum(II,II) paddlewheel complexes bearing non-steroidal anti-inflammatory drug ligands: insights into the chemico-physical profile and first biological assessment. *J. Inorg. Biochem.* 260, 112697. doi:10.1016/j.jinorgbio.2024.112697

Chick, C. N., Takano, M., Eya'ane Meva, F., and Usuki, T. (2025). Synthesis of gold nanoparticles using *Eutrema japonicum* (wasabi): antioxidant and anti-inflammatory studies. *Mater. Adv.* 6, 2365–2370. doi:10.1039/d5ma00065c

de Szalay, S., and Wertz, P. W. (2023). Protective barriers provided by the Epidermis. *Int. J. Mol. Sci.* 24, 3145. doi:10.3390/ijms24043145

Diffey, B. L. (2011). An overview analysis of the time people spend outdoors. *Br. J. Dermatology* 164, 848–854. doi:10.1111/j.1365-2133.2010.10165.x

Gadgil, V. R., Darak, A., Kulkarni, R. A., Patil, S. J., Patil, S. M., Chopada, A., et al. (2023). Recent developments in chemistry of sunscreens and their photostabilization. *J. Indian Chem. Soc.* 100, 100851. doi:10.1016/j.jics.2022.100858

Gonzalez, H., Tarras-Wahlberg, N., Strömdahl, B., Juzeniene, A., Moan, J., Larkö, O., et al. (2007). Photostability of commercial sunscreens upon sun exposure and irradiation by ultraviolet lamps. *BMC Dermatol.* 7, 1. doi:10.1186/1471-5945-7-1

Hartmann, U., and Vahrenkamp, H. (1994). Pyrazolylborat-Zinkkomplexe mit Medikament-Liganden. *Chem. Ber.* 127, 2381–2385. doi:10.1002/cber.19941271207

Heydari, N., Karimi, A. R., Momeni, H. R., Azadikhah, F., and Etemadi, T. (2025). Chitosan Schiff-base hydrogel sunscreen: a multifunctional hybrid network with antioxidant, ultraviolet-shielding, and self-healing properties. *ACS Omega* 10, 8250–8261. doi:10.1021/acsomega.4c09976

Karetsi, V. A., Banti, C. N., Kourkoumelis, N., Papachristodoulou, C., Stalikas, C. D., Raptopoulou, C. P., et al. (2019). An efficient disinfectant, composite material {SLS@$[Zn_3(CitH)_2]$} as ingredient for development of sterilized and non infectious contact lens. *Antibiotics* 8, 213. doi:10.3390/antibiotics8040213

Kaur, C. D., and Saraf, S. (2023). In vitro sun protection factor determination of herbal oils used in cosmetics. *Pharmacognosy Res.* 2, 22–25. doi:10.4103/0974-8490.60586

Kockler, J., Oelgemöller, M., Robertson, S., and Glass, B. D. (2012). Photostability of sunscreens. *J. Photochem. Photobiol. C Photochem. Rev.* 13, 91–110. doi:10.1016/j.jphotochemrev.2011.12.001

Kono, H., Oshima, K., Hashimoto, H., Shimizu, Y., and Tajima, K. (2016). NMR characterization of sodium carboxymethyl cellulose: substituent distribution and mole fraction of monomers in the polymer chains. *Carbohydr. Polym.* 146, 1–9. doi:10.1016/j.carbpol.2016.03.021

Lemoine, P., Viossat, B., Dung, N. H., Tomas, A., Morgant, G., Greenaway, F. T., et al. (2004). Synthesis, crystal structures, and anti-convulsant activities of ternary [ZnII(3,5-diisopropylsalicylate)$_2$], [ZnII(salicylate)$_2$] and [ZnII(aspirinate)$_2$] complexes. *J. Inorg. Biochem.* 98, 1734–1749. doi:10.1016/j.jinorgbio.2004.07.010

Lu, P., Ruan, D., Huang, M., Tian, M., Zhu, K., Gan, Z., et al. (2024). Harnessing the potential of hydrogels for advanced therapeutic applications: current achievements and future directions. *Signal Transduct. Target. Ther.* 9, 166. doi:10.1038/s41392-024-01852-x

Marsh, R. E. (2004). Space group cc: an update. *Acta Crystallogr. Sect. B Struct. Sci.* 60, 252–253. doi:10.1107/s0108768104003878

Palatinus, L., and Chapuis, G. (2007). SUPERFLIP – a computer program for the solution of crystal structures by charge flipping in arbitrary dimensions. *J. Appl. Crystallogr.* 40, 786–790. doi:10.1107/s0021889807029238

Palem, R. R., Kim, B. J., Baek, I., Choi, H., Suneetha, M., Shimoga, G., et al. (2024). *In situ* fabricated ZnO nanostructures within carboxymethyl cellulose-based ternary hydrogels for wound healing applications. *Carbohydr. Polym.* 334, 122020. doi:10.1016/j.carbpol.2024.122020

Pessina, A., Raimondi, A., Cerri, A., Piccirillo, M., Neri, M. G., Croera, C., et al. (2001). High sensitivity of human epidermal keratinocytes (HaCaT) to topoisomerase inhibitors. *Cell. Prolif.* 34, 243–252. doi:10.1046/j.0960-7722.2001.00214.x

Rajamohan, R., Muthuraja, P., Murugavel, K., Mani, M. K., Prabakaran, D. S., Seo, J. H., et al. (2025). Significantly improving the solubility and anti-inflammatory activity of fenofibric acid with native and methyl-substituted beta-cyclodextrins *via* complexation. *Sci. Rep.* 15, 853. doi:10.1038/s41598-024-84745-x

SADABS: Area–Detector Absorption Correction (1996). *Siemens industrial automation*. Madison, WI: Inc.

Sainis, I., Banti, C. N., Owczarzak, A. M., Kyros, L., Kourkoumelis, N., Kubicki, M., et al. (2016). New antibacterial, non-genotoxic materials, derived from the functionalization of the anti-thyroid drug methimazole with silver ions. *J. Inorg. Biochem.* 160, 114–124. doi:10.1016/j.jinorgbio.2015.12.013

Smijs, T. G., and Pavel, S. (2011). Titanium dioxide and zinc oxide nanoparticles in sunscreens: focus on their safety and effectiveness. *Nanotechnol. Sci. Appl.* 4, 95–112. doi:10.2147/nsa.s19419

Stathopoulou, M.-E. K., Banti, C. N., Kourkoumelis, N., Hatzidimitriou, A. G., Kalampounias, A. G., and Hadjikakou, S. K. (2018). Silver complex of salicylic acid and its hydrogel-cream in wound healing chemotherapy. *J. Inorg. Biochem.* 181, 41–55. doi:10.1016/j.jinorgbio.2018.01.004

Tyagi, N., Bhardwaj, A., Srivastava, S. K., Arora, S., Marimuthu, S., Deshmukh, S. K., et al. (2015). Development and characterization of a novel *in vitro* progression model for UVB-Induced skin carcinogenesis. *Sci. Rep.* 5, 13894. doi:10.1038/srep13894